Blurred Image Splicing Localization by Exposing Blur Type Inconsistency

Khosro Bahrami, *Student Member, IEEE*, Alex C. Kot, *Fellow, IEEE*, Leida Li, *Member, IEEE*, and Haoliang Li, *Student Member, IEEE*

***Abstract*— In a tampered blurred image generated by splicing, the spliced region and the original image may have different blur types. Splicing localization in this image is a challenging problem when a forger uses some postprocessing operations as antiforensics to remove the splicing traces anomalies by resizing the tampered image or blurring the spliced region boundary. Such operations remove the artifacts that make detection of splicing difficult. In this paper, we overcome this problem by proposing a novel framework for blurred image splicing localization based on the partial blur type inconsistency. In this framework, after the block-based image partitioning, a local blur type detection feature is extracted from the estimated local blur kernels. The image blocks are classified into out-of-focus or motion blur based on this feature to generate invariant blur type regions. Finally, a fine splicing localization is applied to increase the precision of regions boundary. We can use the blur type differences of the regions to trace the inconsistency for the splicing localization. Our experimental results show the efficiency of the proposed method in the detection and the classification of the out-of-focus and motion blur types. For splicing localization, the result demonstrates that our method works well in detecting the inconsistency in the partial blur types of the tampered images. However, our method can be applied to blurred images only.**

***Index Terms*— Blurred image splicing localization, tampering detection, partial blur type.**

I. Introduction

USING the sophisticated photo-editing softwares, image manipulation can be performed easily and the detection of tampered images is difficult through human vision. Since images can be used in journalism, police investigation and as court evidences, image tampering can be a threat to the security of people and our society. Therefore, detection of image manipulation is an important issue and the development of reliable methods for image integrity examination and image tampering detection is necessary. Image splicing is one of the most common types of image tampering. In splicing of the blurred images, if the original image and the spliced region have different blur types, e.g., out-of-focus and motion, an inconsistency in the blur types of different regions may appear in the tampered image. We focus on detection of such kind of inconsistency for splicing localization in a blurred image. However, the forger may remove the anomaly introduced by the traces of splicing and make the image visually pleasant by some post-processing operations such as resizing the tampered image into a smaller size or blurring the spliced region boundary. Such operations remove the artifacts used by many existing techniques to make the detection of splicing difficult. In this paper, we address this problem by targeting the partial blur type inconsistency detection which is almost robust to such kind of operations.

(a) (b)

Fig. 1. (a) An authentic image with out-of-focus blur. (b) A tampered image generated by splicing a motion blurred region in image (a), which has inconsistent blur types in the right side (motion blur) and left side (out-of-focus blur).

Fig.1 (a) shows an authentic image with out-of-focus blur and (b) a tampered image generated by splicing a motion blurred region in image (a). The tampered image (b) has two different partial blur types, one on the left and one on the right side. The right side (spliced region) with motion blur indicates the camera movement with respect to the scene while the left side (original image) has the out-of-focus blur. Since the objects (walls and building) in these regions are stationary, such inconsistency in the blur types can be used for splicing localization. In this paper, the objective is the localization of the spliced region in a tampered blurred image by exploration the inconsistency in the partial blur types.

Natural blur types in an image can be out-of-focus or motion blur. Out-of-focus blur is caused by the placement of an object out of camera depth of field or incorrect focal length setting. Motion blur is generated due to motion of the camera or the object. Besides, it is very common that someone blurs a region of an image artificially by some photo editing tools. In both natural and artificial blur, the simplest form of motion and out-of-focus blur kernels are specified by linear

Manuscript received September 21, 2014; accepted January 5, 2015. Date of publication January 20, 2015; date of current version March 7, 2015. This work was carried out at the Rapid-Rich Object Search (ROSE) Lab at the Nanyang Technological University, Singapore. The ROSE Lab is supported by a grant from the Singapore National Research Foundation and administered by the Interactive and Digital Media Programme Office at the Media Development Authority. The associate editor coordinating the review of this manuscript and approving it for publication was Dr. Teddy Furon.

K. Bahrami, A. C. Kot, and H. Li are with the School of Electrical and Electronic Engineering, Nanyang Technological University, Singapore 639798 (e-mail: khosro1@ntu.edu.sg; eackot@ntu.edu.sg; hli016@ntu.edu.sg).

L. Li is with the School of Information and Electrical Engineering, China University of Mining and Technology, Xuzhou 221116, China (e-mail: reader1104@hotmail.com).

Color versions of one or more of the figures in this paper are available online at http://ieeexplore.ieee.org.

Digital Object Identifier 10.1109/TIFS.2015.2394231

1556-6013 © 2015 IEEE. Personal use is permitted, but republication/redistribution requires IEEE permission.
See http://www.ieee.org/publications_standards/publications/rights/index.html for more information.

motion and cylinder disk, respectively. These blur kernels can be defined by parametric models. However, in practice, the motion blur could be non-linear [1], [2], and out-of-focus blur could be asymmetric shape [3] which are considered to be non-parametric and more complex. There are some works done [1]–[9] on non-parametric blurs in blur kernel estimation and debluring areas. However, less works have been done for blur type detection and classification for such complex forms. In this paper, we consider parametric as well as non-parametric forms of motion and out-of-focus blurs which are more realistic in image forensics applications.

The rest of this paper is organized as follows. A brief review of image splicing localization techniques and partial blur type detection methods are presented in section II. In section III, blur type detection features are proposed for out-of-focus/motion blur type classification. By incorporating such features, we propose in section IV, a partial blur type detection and classification framework used for splicing localization in blurred images. Experimental results are shown in section V. Section VI concludes and discusses the paper.

II. Related Work

Since we focus on splicing localization based on blur type inconsistency, in this section, we categorize the related works into image splicing localization and partial blur type detection approaches. The existing techniques of splicing localization in a tampered image [10] can be categorized into (1) format-based such as DJPG compression detection [11]; (2) camera-based such as demosaicing regularity [12]–[14], camera response function [15] and sensor pattern noise [16]; (3) pixel-based such as re-sampling [17], [18], contrast enhancement detection [19] and local descriptors [20], [21]; (4) physically-based such as light anomalies [22] and size inconsistencies [23]. The method [21] has been proposed for steganalysis, while the recent research in steganalysis and splicing detection shows a close relation in these two areas [20]. Therefore, the method [21] can be used in a block-based fashion for splicing localization.

These techniques have some limitations in splicing localization in a tampered blurred image when some post-processing operations are applied. For instance, resizing the tampered image and artificial blurring of the spliced region boundary, can be an anti-forensics threat that may remove the artifacts used by such techniques. The light anomalies [22], size inconsistencies [23] and sensor pattern noise [16] are more robust to such post processing operations. However, the light anomalies [22] only works in the case of lightning inconsistency, the size inconsistencies [23] is applicable when the actual size of objects is available and sensor pattern noise [16] requires the knowledge of camera photo-response non-uniformity noise information. On the contrary, splicing detection based on blur inconsistency has its advantages. Such detection is robust to image resizing and spliced region boundary blurring and does not need camera information. This motivates us to propose a method based on partial blur type inconsistency analysis. However, our method can be applied to blurred images only. Besides, each technique works when there is a specific assumption. Usually image splicing detection system involves the incorporation of a large set of techniques to examine various splicing artifacts.

Some works [24]–[31] have been proposed for image tampering detection based on blurriness inconsistency within the image. However, these methods only work for blur degree inconsistency but not for images with multiple blur types. Kakar *et al.* [32] proposed a method for splicing detection based on the inconsistency in the blurriness and direction of motion blur. By applying this method for discrimination of motion and out-of-focus blur, it still generates a direction for out-of-focus blur which is random based on the image content. Therefore, it cannot be used to discriminate motion and out-of-focus blur. In addition, this method only works for linear motion blur and it cannot be applied to the more complicated motion blur kernels.

Some works have been done for partial blur type detection and classification. For example, Chen *et al.* [33] proposed a method based on the lowest directional high-frequency energy to classify motion and out-of-focus blurs. Liu *et al.* [34] used the correlation of shifted blocks as a feature for motion and out-of-focus blurs classification. Su *et al.* [35] proposed a method for the segmentation of motion and out-of-focus blurred regions in the partial blurred images based on alpha channel feature. Aizenberg *et al.* [36] proposed a method for segmentation of motion, gaussian and uniform blurs based on the magnitude of cepstrum coefficients. However, for partial blur type detection, these methods may not be practical due to an overly simplified assumption on the motion blur. Direction of the motion blur is the main consideration to classify motion and out-of-focus in these methods, while in practice the motion blur may not be a simple line. Since the motion of the camera or the objects can be complicated, the motion blur can have a complex form which is what we consider in this paper. In addition, the blur type detection for an image block is affected by the size of the block and the blur degree which are not addressed in these methods.

Our initial thoughts in splicing localization by checking blur type inconsistency can be found in [37]. In this paper, we consider more general types of motion and out-of-focus blurs including both parametric and no-parametric blur kernels. We also propose a different sets of features for local blur detection so that our method is able to detect a wider range of blur kernels. We formulate a blur type classifier by incorporating the proposed features instead of using a predefined set of blur kernels. We apply a fine splicing localization technique to increase the precision of boundary for the regions. We evaluate the proposed method by considering different scenarios with larger databases of images.

In the next section, we propose a set of features for blur type detection, used for classification of the image blocks into out-of-focus/motion blur. Such features work well for both simple and complex forms of motion as well as out-of-focus blurs.

III. Blur Type Detection Features

As mentioned earlier, the out-of-focus and motion blur kernels can be represented in parametric or non-parametric categories. In the parametric category, we consider the linear

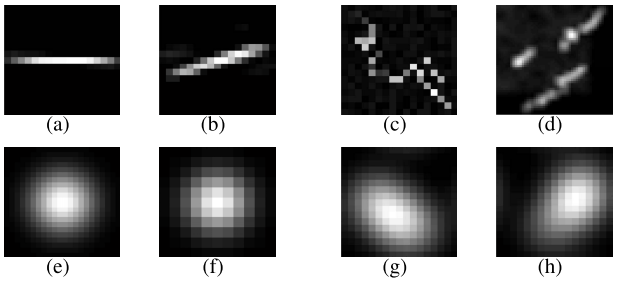

Fig. 2. Examples of blur kernels: (a) and (b) parametric motion (linear); (c) and (d) non-parametric motion (non-linear); (e) and (f) parametric out-of-focus (symmetric); (g) and (h) non-parametric out-of-focus (asymmetric).

motion blur described by length L and direction θ and symmetric out-of-focus described by a cylinder disk with radius R. In the non-parametric category, we consider the motion blur to be non-linear or with multiple directions and the out-of-focus blur to be asymmetric. We define this category in a 2D matrix with random values. Fig. 2 shows the top view of some blur kernel examples with brighter regions indicating larger values.

We observe that despite of the kernel size, motion blur kernels tend to be sparse because most values in these kernels are close to zero (dark regions) while out-of-focus blur kernels are less sparse. Fig. 3 (a)-(h) show the pixel value distributions of the blur kernels in Fig. 2 (a)-(h), respectively, which reveal the number of blur kernel values at different intensity values. To generate these distributions, all local blur kernels are resized to 100×100, followed by scaling the sum of the kernel values of each kernel into 1. From these distributions, we observe that out-of-focus and motion blur kernels have different statistics. We use such differences to extract a set of features by describing the blur kernel distributions roughly with Generalized Gaussian Distribution (GGD) below.

$$f(\mathbf{K};\mu,\gamma,\sigma) = \left(\frac{\gamma}{2\sigma\Gamma(\frac{1}{\gamma})\sqrt{\frac{\Gamma(\frac{1}{\gamma})}{\Gamma(\frac{3}{\gamma})}}}\right) e^{-\left(\frac{|\mathbf{K}-\mu|}{\sigma\sqrt{\frac{\Gamma(\frac{1}{\gamma})}{\Gamma(\frac{3}{\gamma})}}}\right)^{\gamma}} \quad (1)$$

where $\mathbf{K}$ is the blur kernel estimated from a given region, $\Gamma(.)$ is the gamma function, μ is the mean, σ is the standard deviation and γ ($\gamma > 0$) is the shape-parameter of the GGD. We calculate the value of γ and σ for the blur kernel distributions shown in Fig. 3 using the method proposed in [38]. The values of γ and σ suggest distinctive difference in value for the out-of-focus blur kernels vs. motion blur kernels. To further explore the values of γ and σ for different blur kernel types, we plot in Fig. 4 the 2D scatter plot of γ versus σ for the blur kernels estimated from a set of randomly selected 1200 (600 out-of-focus and 600 motion) blurred images. The estimated blur kernels include a variety of blur kernels such as linear motion, non-linear motion, multi line motion due to hand shake, objects motion, camera motion, and also symmetric and asymmetric out-of-focus blur kernels. Regardless of the blur kernel is simple or complex, the value of γ in the out-of-focus blur kernels is larger than the motion blur kernels, while σ in the out-of-focus blur kernels is smaller than motion blur kernels. Such scatter plot shows that these two classes of kernels from motion and out-of-focus can easily be separable. Below, we describe our proposed framework which employs these features for partial blur type detection used in splicing localization.

IV. Proposed Framework

The proposed framework for splicing localization shown in Fig. 5 are carried out in three steps here. First, we propose local blur type features (block-based blur type features) generated by partitioning an input tampered image into blocks. Second, we formulate a classifier to classify the image blocks into out-of-focus or motion blur types, based on the proposed features. Third, we apply an energy based method for the fine splicing localization by increasing the boundaries precision from block to pixel level. Due to the blur degree or the image content, the detection of different blur types in a spliced image is not easy with the human vision. The proposed framework can be used to discriminate out-of-focus and motion blur types in an image. We may detect inconsistency in the partial blur types and the semantic content of the regions for splicing localization. The following sections provide detailed steps in this proposed framework.

A. Local Blur Type Feature Extraction

In the step shown in Fig. 5(a), the objective is to extract local blur type features of an input blurred image with possible spliced region. The image is partitioned into blocks and the blur kernels of the image blocks, denoted as local blur kernels, are estimated. Given a color image $\mathbf{B}$ of size $M \times N$, we convert into a gray scale image $\mathbf{G}$ and then partition $\mathbf{G}$ into blocks $\mathbf{G}_{i,j}$ with $L \times L$ pixels and d ($d < L$) pixels overlapping, where i and j are the index for different blocks ($1 \le i \le \lfloor \frac{M}{L-d} \rfloor$, $1 \le j \le \lfloor \frac{N}{L-d} \rfloor$). For an image block $\mathbf{G}_{i,j}$, the image blurring process is given by

$$\mathbf{G}_{i,j} = \mathbf{I}_{i,j} * \mathbf{K}_{i,j} + \mathbf{N}_{i,j} \quad (2)$$

where $\mathbf{I}_{i,j}$ represents a sharp image block, $\mathbf{K}_{i,j}$ is a local blur kernel represented by a two-dimensional matrix with size of $\kappa \times \kappa$, $\mathbf{N}_{i,j}$ is the noise matrix and '$*$' denotes convolution.

To estimate $\mathbf{K}_{i,j}$ from $\mathbf{G}_{i,j}$, previous techniques [4]–[9], [39]–[44] perform blur kernel estimation based on Blind Image Deconvolution (BID). Among these techniques, some work well for the specific blur type, and some are applicable for the whole image blur kernel estimation. Considering a method that is independent of the blur type and applicable for small patches, we use the method in [39] to estimate all local blur kernels $\mathbf{K}_{i,j}$ of the image $\mathbf{G}$. This method formulates the BID in a Bayesian framework and searches for the blur kernel of the blurred image using a maximum a posteriori (MAP) technique. It formulates the problem in derivative space and assumes prior models for the image, blur kernel and noise. Finally, an expectation-maximization framework is used to estimate the blur kernel by optimizing the MAP.

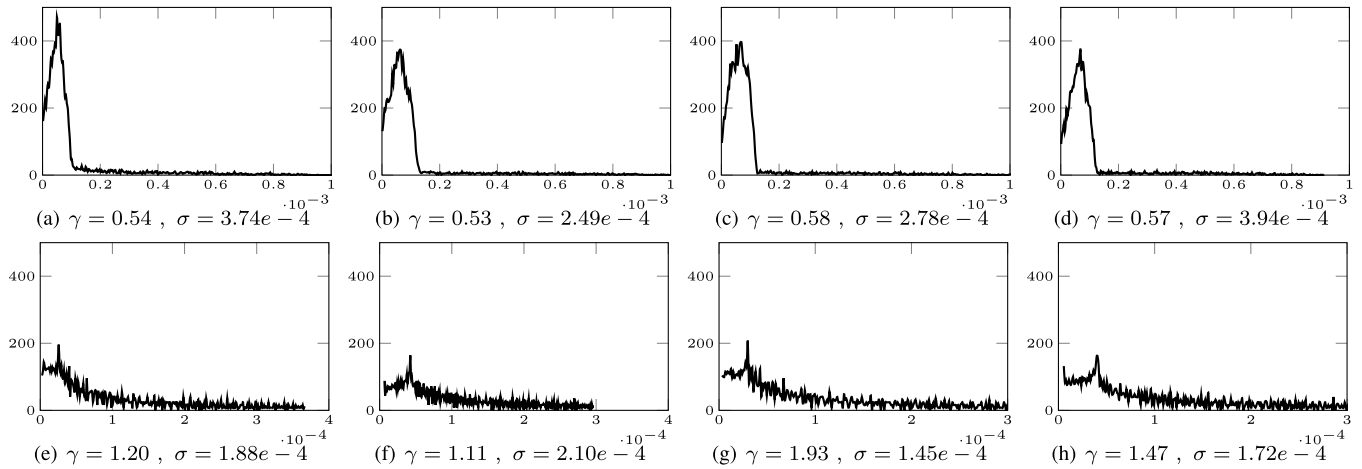

Fig. 3. Pixel value distributions estimated from (a) and (b) linear motion; (c) and (d) non-linear motion; (e) and (f) symmetric out-of-focus and (g) and (h) asymmetric out-of-focus blur kernels in Fig. 2.

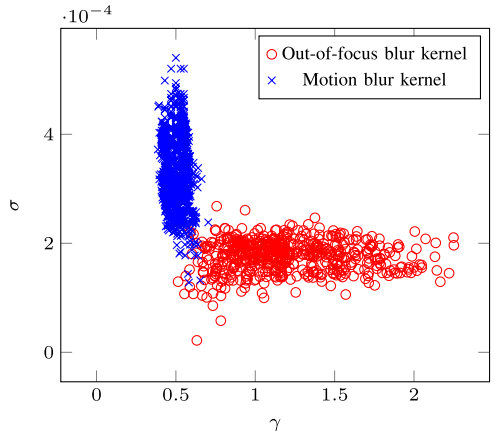

Fig. 4. 2D scatter plot of γ vs σ for Generalized Gaussian Distribution of the blur kernels estimated from 600 out-of-focus and 600 motion blurred images.

As mentioned before, the distributions of the out-of-focus and motion blur kernels have different statistics. Based on the study carried out in section III, γ and σ can be used as features for blur type classification. We propose these features for local blur type detection by describing the local blur kernels $\mathbf{K}_{i,j}$ with GGD by replacing $\mathbf{K}$ with $\mathbf{K}_{i,j}$ in Eq. (1). As such, the shape-parameter $\gamma_{i,j}$ and standard deviation $\sigma_{i,j}$, representing blur type features at block level, are used in the next section for blur type classification.

B. Blur Type Detection and Classification

In this section, we incorporate the proposed blur type features to classify the blur type of image block $G_{i,j}$ into out-of-focus or motion. We generate a new feature $\nu_{i,j}$ by combining $\gamma_{i,j}$ and $\sigma_{i,j}$ for dimensionality reduction. By representing $\gamma_{i,j}$ and $\sigma_{i,j}$ as the feature vector $\mathbf{x}_{i,j} = [\gamma_{i,j}\ \sigma_{i,j}]^T$, we define a mapping $\nu_{i,j} = f(\mathbf{x}_{i,j})$. In general, the optimal mapping $\nu_{i,j} = f(\mathbf{x}_{i,j})$ is a non-linear function. Since there is no systematic way to generate non-linear transform, we reduce the dimensionality based on linear transform of LDA [45], to yield

$$\nu_{i,j} = \mathbf{w}^T \mathbf{x}_{i,j} = [w_\gamma\ \ w_\sigma][\gamma_{i,j}\ \sigma_{i,j}]^T \tag{3}$$

where $\mathbf{w} = [w_\gamma\ \ w_\sigma]^T$ is the vector which projects the γ- and σ-axis onto a line. To find the best projection, the Fisher linear discriminant [45] suggests maximizing between-class scatter and minimizing the within-class scatter. Applying this rule for two classes of out-of-focus and motion blurs, yields

$$\mathbf{w} = {\mathbf{S}_w}^{-1}(\mathbf{e}_O - \mathbf{e}_M) \tag{4}$$

where $\mathbf{e}_O = [e_{\gamma_O}\ e_{\sigma_O}]^T$ and $\mathbf{e}_M = [e_{\gamma_M}\ e_{\sigma_M}]^T$ are the vectors of the mean of $\gamma_{i,j}$ and $\sigma_{i,j}$ in out-of-focus and motion blur classes, respectively, and $\mathbf{S}_w$ is the within-class scatter matrix obtained from

$$\mathbf{S}_w = \mathbf{S}_O + \mathbf{S}_M \tag{5}$$

where $\mathbf{S}_O$ and $\mathbf{S}_M$ are the variances of $\gamma_{i,j}$ and $\sigma_{i,j}$ in out-of-focus and motion blur classes, respectively. Using the generated feature, $\nu_{i,j}$, we formulate a binary classifier to classify the blur type of the image block $\mathbf{G}_{i,j}$, denoted as $B_{i,j}$, as out-of-focus or motion, where

$$B_{i,j} = \begin{cases} \text{'M' (motion blur),} & \text{if } \nu_{i,j} \geq \rho \\ \text{'O' (out-of-focus blur),} & \text{otherwise} \end{cases} \tag{6}$$

and ρ is the threshold that discriminates the blur type of an image block into out-of-focus or motion.

By defining two classes including out-of-focus blur as the positive class and motion blur as the negative class, the true positive rate (TPR) and true negative rate (TNR) are the detection accuracy of out-of-focus blur and motion blur regions, respectively. The threshold ρ is chosen in such a way to maximize the average of TPR and TNR on a training set of images. Also, to calculate the projection vector $\mathbf{w}$, we use the training set of out-of-focus and motion blurred images. Using the calculated ρ and $\mathbf{w}$, we measure the performance for the testing set.

Since the blocks without content (smooth blocks) are not reliable in blur type detection, the image blocks are categorized into smooth and non-smooth using the method in [46].

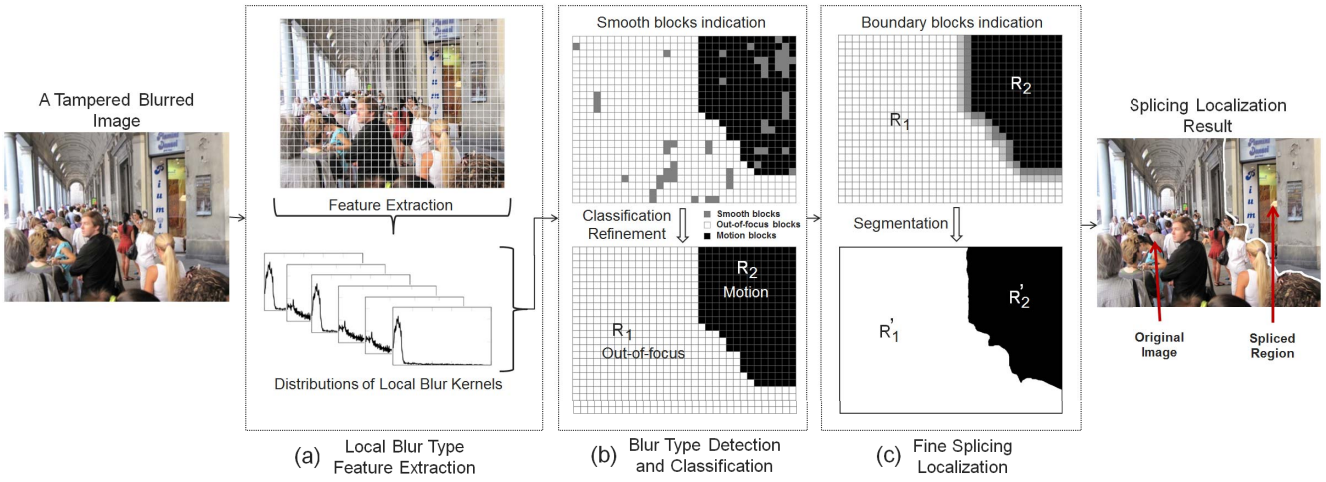

Fig. 5. Proposed Framework for Blurred Image Splicing Localization.

In this method, a sobel edge detector is first used to indicate the edge pixels. Then each block is categorized into smooth or non-smooth based on the number of edge pixels. If the number of edge pixels is larger than a threshold, the block is considered as non-smooth otherwise it is a smooth block. For a 64×64 block, the threshold is chosen to be 0.2% of the total number of pixels in the block.

The smooth blocks are shown in Fig. 5 (b) in gray color. After the blur type classification, a refinement is applied to classify the smooth blocks based on the blur type of the nearest non-smooth ones. If a smooth block has more than one nearest non-smooth block with different blur types, the majority of blur types indicates the blur type of the smooth block. For the tampered image shown in Fig. 5, step (b) shows the classification result of the image blocks before and after refinement where all blocks are classified into out-of-focus or motion blur. Such a classification discriminates the image into s regions $R_1, R_2, ..., R_s$, where s may change from 2 to $\lfloor \frac{M}{L-d} \rfloor \times \lfloor \frac{N}{L-d} \rfloor$ (the number of image blocks).

C. Fine Splicing Localization

After the generation of s regions $R_1, R_2, ..., R_s$, we increase the boundary precision of the regions to pixel level. First, we define boundary blocks as the ones which at least one of their 4-neighbors are from a different region. As an example, for two regions R_1 and R_2 shown in Fig. 5(c) with white and black colors, respectively, the boundary blocks are indicated in gray color. Second, we assign the labels '1', '2', ..., 's' to the pixels of all non-boundary blocks in the regions $R_1, R_2, ..., R_s$, respectively. The remaining pixels of the boundary blocks are non-labeled.

Third, we apply an energy-based technique [47] to propagate the labels from labeled pixels to non-labeled pixels by interpolation. Using the matting Laplacian, the interpolation problem can be formulated by minimizing a cost function. This cost function considers pixels intensity in addition to the labels to discriminate the pixels based on the different intensities. Since it is likely that the intensity of the pixels around the boundary of the spliced region and the original image are different, by considering the pixels intensity, a fine boundary localization can be achieved. After assigning the labels to all pixels of the boundary blocks, we generate the regions $R'_1, R'_2, ..., R'_s$ from the corresponding pixels. An example of such fine localization is shown in Fig. 5(c).

After generation of $R'_1, R'_2, ..., R'_s$, a human decision is needed to indicate the spliced region based on the some inconsistencies between the blur type and semantic of the image. Such inconsistencies can be discovered based on the following facts to detect possible forgery:

1) In an image with out-of-focus blur, the stationary objects, e.g. building, should not have motion blur.
2) In an image with hand shaking or camera motion blur, all the objects should have motion blur, unless the object is stationary with respect to the camera.

In such a case, the spliced region and the original image are differentiated by the blur type regions. For instance, for the image shown in Fig. 5, since the objects (walls and building) are stationary while the blur types are different, we detect the regions as original and spliced regions.

V. Experimental Results

In this section, we evaluate the performance of the proposed method for splicing localization by considering different scenarios, such as various blur degrees, natural/ artificial blur, presence of post-processing operations and different tampered region sizes.

A. Performance Evaluation for Splicing Localization

In the following two experiments, we examine our method for splicing localization when the original image and the spliced region have different natural blur types.

In the first experiment, we compare our method with some of the state-of-the-art methods in partial blur type detection, including Chen *et al.* [33], Su *et al.* [35] and Aizenberg *et al.* [36]. We took 1200 natural blurred photos (600 out-of-focus and 600 motion) in TIFF noncompressed

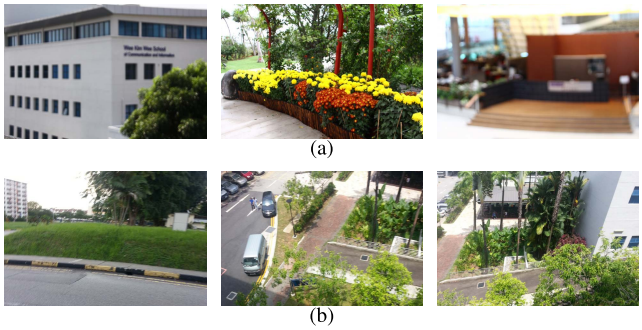

Fig. 6. Some examples of (a) out-of-focus blur and (b) motion blur images in dataset.

format with size of ranging from 1024 × 768 to 3456 × 2304 pixels, from 4 cameras, including Canon EOS 50D, Canon EOS 60D, Nikon D50 and Sony NEX-5N. The ground truth of motion vs out-of-focus blurs being recorded properly. To generate the motion blurred images, we create motion with the camera in various degrees when taking pictures. To generate the out-of-focus blurred images, we took the blurred photos by using the manual focusing in various degrees. When taking the out-of-focus blurred photos, the camera was mounted onto the tripod stand to ensure maximum stability so that the cause of the natural blur was only due to the manual focusing controlled by the user. Some examples of the dataset are shown in Fig. 6. By randomly choosing 1200 pairs of the out-of-focus and motion blurred images and splicing each pair, we create 1200 multi-type blurred images. Splicing is performed by some predefined masks in which almost half of each image has out-of-focus and another half has motion blur with irregular splicing boundary.

We extract local blur type features of the blocks of all the images by considering three schemes regarding the block size, including non-overlapping blocks of size 64×64, overlapping blocks of size 64×64 with 32 pixels overlapping (denoted as 64×64^w), and overlapping blocks of size 128×128 with 64 pixels overlapping (denoted as 128×128^w). Out of 1200 images, 600 images are randomly selected for training and the rest are for testing. We define two classes including out-of-focus blur as the positive class and motion blur as the negative class. To classify the image pixels into out-of-focus or motion blur types, we incorporate the classifier in Eq. (6) for classification of the image blocks. Table I shows a performance comparison. Our average accuracy for block size of 64×64, 64×64^w, 128×128^w outperforms other methods. In our method, among the different schemes, 64×64^w shows better accuracy which we consider in the next experiments.

In the second experiment, we examine the proposed framework in splicing localization by considering different spliced region sizes including 100×100, 200×200 and 512×384 and whole image size of 1024×768 cropped from the original blurred images. We create datasets of tampered images exhibiting blur type inconsistency by splicing the regions extracted from 600 motion blurred images in 600 out-of-focus blurred images, and the regions extracted from 600 out-of-focus blurred images in 600 motion blurred images, at random locations. As such, we have 1200 tampered images for each tampered region size. The tampered regions are defined as irregular shapes. It is worth to note that, since in this scenario we consider the natural blurred images, the original image and the spliced region may have any blur degree. We define two classes including spliced region as the positive class and authentic region as the negative class, used in the rest of this paper to evaluate the splicing localization performance. Table II shows the performances comparison. Our method outperforms the prior works [33], [35], [36] for different spliced region sizes. It can be seen that the performance of our method does not vary much by decreasing the size of tampered region due to the block overlapping scheme we incorporated.

TABLE I

COMPARISON OF THE METHODS FOR BLUR TYPE CLASSIFICATION IN IMAGES WITH HALF NATURAL OUT-OF-FOCUS AND HALF NATURAL MOTION BLUR BY CONSIDERING BLOCKS OF SIZE 64×64, 64×64^w (64×64 WITH 32 PIXELS OVERLAPPING) AND 128×128^w (128×128 WITH 64 PIXELS OVERLAPPING)

Method	Scheme	Block Size	TPR (%)	TNR (%)	Accuracy (%)
Chen *et al.* [33]	Non-overlapping	64×64	82.4	81.1	81.7
	Overlapping	64×64^w	83.6	80.0	81.8
		128×128^w	78.7	79.3	79.0
Su *et al.* [35]	Non-overlapping	64×64	80.2	82.1	81.2
	Overlapping	64×64^w	85.1	83.5	84.3
		128×128^w	82.8	83.2	83.0
Aizenburg *et al.* [36]	Non-overlapping	64×64	57.2	54.2	55.7
	Overlapping	64×64^w	53.7	58.4	56.1
		128×128^w	84.1	83.7	83.9
Proposed Method	Non-overlapping	64×64	93.2	92.4	92.8
	Overlapping	64×64^w	94.5	94.2	94.3
		128×128^w	90.6	92.0	91.3

TABLE II

PERFORMANCE COMPARISON OF THE METHODS FOR SPLICING LOCALIZATION BY CONSIDERING IMAGE SIZE OF 1024×768 PIXELS AND SPLICED REGION SIZES OF 100×100, 200×200 AND 512×384

Method	Spliced Region Size	TPR(%)	TNR(%)	Accuracy(%)
Chen *et al.* [33]	100×100	80.1	82.4	82.3
	200×200	85.8	84.0	84.1
	512×384	83.1	84.7	84.3
Su *et al.* [35]	100×100	80.3	82.7	82.6
	200×200	83.4	85.8	85.7
	512×384	82.5	84.2	83.8
Aizenburg *et al.* [36]	100×100	83.2	86.3	86.2
	200×200	81.0	85.2	85.0
	512×384	86.3	83.8	84.4
Proposed Method	100×100	94.1	95.4	95.3
	200×200	93.8	96.1	96.0
	512×384	95.9	95.2	95.4

B. Reliability to Resizing and Splicing Boundary Blurring

In this experiment, we show the effect of post-processing operation (blurring the splicing boundary following by resizing) on the performance of our method and some of the state-of-the-art methods in splicing localization, including JPEG artifacts [11], CFA artifacts [12] and local descriptors (LD) [21]. We generate the tampered images similar to the previous experiment, while the spliced region is considered to be 10% and 30% of the tampered image size. To prepare the dataset to examine JPEG artifacts [11], the authentic region is

TABLE III
EFFECT OF POST-PROCESSING OPERATIONS (BLURRING THE SPLICING BOUNDARY FOLLOWED BY TAMPERED IMAGE RESIZING) ON THE PERFORMANCE OF THE STATE-OF-THE-ART SPLICING LOCALIZATION METHODS AND OUR PROPOSED METHOD

JPEG artifacts method [11] (QF1=90, QF2=100)						
Spliced Region Size (%)	10			30		
Resizing Rate (%)	100	90	50	100	90	50
TPR (%)	68.4	50.1	48.2	63.2	51.3	44.2
TNR (%)	66.5	52.6	49.7	60.5	49.1	46.5
Accuracy (%)	66.6	52.5	49.6	61.0	49.4	45.9
JPEG artifacts method [11] (QF1=50, QF2=90)						
Spliced Region Size (%)	10			30		
Resizing Rate (%)	100	90	50	100	90	50
TPR (%)	87.4	53.3	51.4	88.3	53.8	56.2
TNR (%)	89.2	58.3	54.7	87.2	50.3	51.6
Accuracy (%)	89.0	57.8	54.4	87.5	51.4	53.0
CFA artifacts method [12]						
Spliced Region Size (%)	10			30		
Resizing Rate (%)	100	90	50	100	90	50
TPR (%)	89.9	61.3	49.9	92.1	62.1	50.6
TNR (%)	90.8	67.5	54.2	91.5	63.3	49.1
Accuracy (%)	90.7	66.9	53.7	91.7	63.0	49.6
Local Descriptors method [21]						
Spliced Region Size (%)	10			30		
Resizing Rate (%)	100	90	50	100	90	50
TPR (%)	85.2	43.2	38.4	76.2	48.2	34.2
TNR (%)	78.1	39.9	39.4	82.0	38.5	36.2
Accuracy (%)	78.8	40.2	39.3	80.0	41.6	35.6
Our method						
Spliced Region Size (%)	10			30		
Resizing Rate (%)	100	90	50	100	90	50
TPR (%)	93.5	92.4	92.5	94.3	93.2	94.1
TNR (%)	95.2	94.8	93.4	96.0	95.4	94.7
Accuracy (%)	95.0	94.6	93.3	95.4	94.7	94.5

JPEG compressed with quality factor of QF_1. After splicing, the whole tampered image is JPEG compressed with quality factor of QF_2, resulting in having the traces of single and double compression in the spliced region and authentic region, respectively. We choose two quality factors ($QF_1 = 90$, $QF_2 = 100$) with small different and two quality factors ($QF_1 = 50$, $QF_2 = 90$) with bigger different to create weak and strong traces for JPEG artifacts, respectively. To prepare the dataset to examine CFA artifacts [12], the CFA artifacts of the spliced region is removed while the CFA of the authentic region is reinterpolated using gradient-based demosaicking algorithm, as described in [12].

To show the effect of post-processing operations on the performance of some of the state-of-the-art methods, we first assume that there is no post-processing operations (indicated by Resizing Rate = 100%). Then, we blur the splicing boundary to remove the splicing traces, followed by resizing the tampered images into 90% (Resizing Rate = 90%) and 50% (Resizing Rate = 50%) of the original image size, as shown in Table. III.

We use half of the images for training and another half for testing to measure the performance of the methods [11], [12], [21]. By defining two classes including spliced region as the positive class and the original image as the negative class, the TPR and TNR are the detection accuracy of the spliced region and the original image, respectively. Table. III shows the effect of post-processing operation (blurring the splicing boundary following by resizing) on the performance of our method and previous methods. The result shows that even in the presence of post processing operations our method has high performance, indicating reliability to splicing boundary blurring and resizing, while the previous methods have low performance.

We show an example in Fig. 7 the result of our method and previous methods [11], [12], [21] for the tampered images shown in Fig. 7 (b) and (h). Fig. 7 (a) shows an authentic out-of-focus blurred image. By splicing a motion blurred region in image (a), a tampered image is generated with size of 1600×1200, in Fig. 7 (b). Fig. 7 (h) shows another tampered image with size of 2048×1536 generated by splicing an out-of-focus blurred region in an authentic motion blurred image shown in Fig. 7 (g). After splicing, both tampered images are post-processed by artificial blurring of the spliced region boundary followed by resizing into 1024×768 pixels.

The binary splicing localization maps generated by the methods [11], [12], [21] for the images (b) and (h) are shown in Fig. 7 (c)-(e) and (i)-(k), respectively, where the white pixels indicate the possibly tampered areas. To generate such binary maps, the generated probability maps (gray scale maps) using [11], [12], [21] are binarized with the threshold ρ which is chosen in such a way to maximize the average of TPR and TNR on the training set of images. For the generated probability maps using [11], [12], [21], the values between 0 and 1 show the probability that splicing occurs. By setting the threshold ρ, the values are classified into the spliced or the authentic regions, indicated by white and black color, respectively. If a value is larger than the threshold, it belongs to the spliced region, or vise versa.

The results reveal that these methods cannot detect the spliced region. Artificial blurring of the spliced region removes the traces of splicing used by [21] and image resizing removes the artifacts used by the CFA [12] and JPEG [11] methods. Therefore, such techniques may not detect the spliced region while our method is more reliable to such post-processing operations. The result of our method shown in Fig. 7 (f) and (l) discriminates the image into out-of-focus and motion blur type regions, indicated in white and black, respectively. Such a discrimination indicates spliced and authentic regions with different blur types.

C. Localization of Artificially Blurred Spliced Region

In this section, we evaluate our method in splicing localization when the original image has the natural blur and the spliced region has the artificial blur. For instance, the original image has natural motion blur due to the camera motion while the forger splices a region from a sharp image in the original image. In such a case, the forger should blur the spliced region artificially to make the tampering more convincing. However, detection of blur type of the original image may not be easy by human vision. When the blur type of the spliced region and the original image are different, the inconsistency in the blur types can be used to locate the tampered region. Since the forger may use parametric (simple form) or non-parametric (complex form) blur kernels to blur the tampered region, two different cases are discussed in the following.

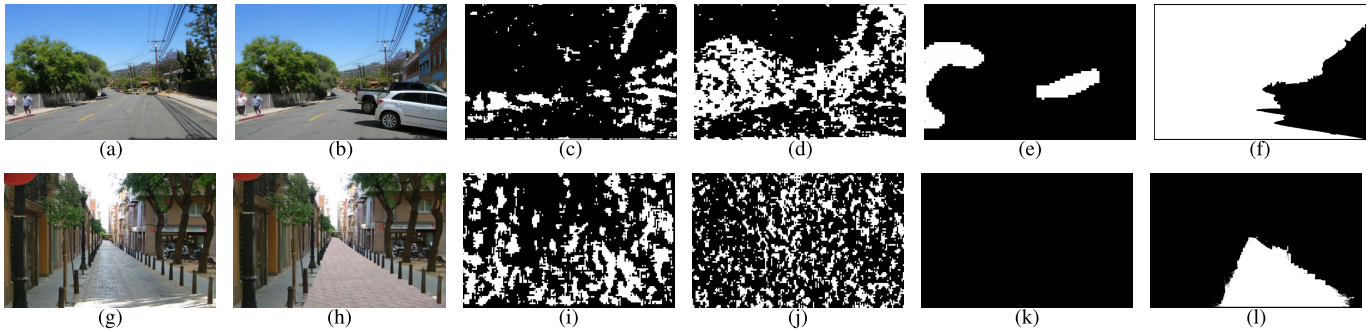

Fig. 7. Example of splicing localization in the presence of post processing operations (spliced region boundary blurring followed by resizing). (a) An authentic out-of-focus blurred image. (b) A tampered image generated by splicing a motion blurred region in image (a), followed by post processing operations. (g) An authentic motion blurred image. (h) A tampered image generated by splicing an out-of-focus blurred region in image (g), followed by post processing operations. Binary splicing localization maps generated by (c) and (i) CFA artifacts [12]; (d) and (j) JPEG artifacts [11]; (e) and (k) local descriptor [21]; where white pixels indicate high possibility tampered areas. (f) and (l) show the results of our method in detection of inconsistent blur types (out-of-focus and motion blur type regions are indicated by white and black regions, respectively) used for splicing localization.

Fig. 8. Some examples of sharp images.

1) The Spliced Region Is Blurred by Parametric Blur Kernel: In this case, we assume that the forger uses parametric blur kernels to blur the tampered region. We compare the performance of our method with [33], [35], and [36] by considering various blur degrees. We create datasets of tampered images by replacing a region of 600 natural out-of-focus blurred images with sharp regions blurred with a set of parametric motion blur kernels. Also, we replace a region of 600 natural motion blurred images with sharp regions blurred with a set of parametric out-of-focus blur kernels. The spliced regions are chosen to be irregular shapes with size of ranging from 100×100 to 300×300 pixels, extracted with random spatial alignment from a set of 1200 sharp images. The sharp images are collected from Flicker website [48] with size of ranging from 800×600 to 4416×3312 pixels in JPEG format. To make sure that the collected images are not blur, we verify the sharpness of each image based on human vision. Examples of sharp images are shown in Fig. 8.

The spliced regions are blurred to create three datasets P_1, P_2, and P_3 with different blur degrees listed in Table IV. As such, we generate 1200 tampered images for each dataset. The range of blur degrees are chosen to be increased from P_1 to P_3. In each dataset, each image is blurred randomly with a blur degree. The whole range of blur degrees for our-of-focus and motion blurs are $2 \leq R \leq 14$ and $2 \leq L \leq 26$, respectively. The lower bound of blur degrees are chosen as $R = 2$ and $L = 2$, where the blur degree is negligible. The upper bound of blur degrees are chosen as $R = 14$ and $L = 26$ due to the size of image blocks. Usually the size of estimated blur kernel should be smaller than half of the image block size. For instance, to estimate the local blur kernel of an image block with size of 64 pixels, the size of blur kernel should be less than 32 ($\frac{64}{2}$) pixels. Therefore, these upper limits are chosen to make sure that the size of estimated blur kernel is enough to estimate the blur accurately. However, if higher blur degrees are desired, larger block and kernel size should be chosen in the cost of dropping the accuracy.

TABLE IV

DATABASES OF TAMPERED IMAGES WHEN THE SPLICED REGIONS HAVE VARIOUS BLUR DEGREES (ORIGINAL IMAGE HAS NATURAL BLUR WHILE THE SPLICED REGION HAS ARTIFICIAL BLUR)

Datasets	# of Images	Blur Degree of Out-of-focus Blurred Region (R)	Blur Degree of Motion Blurred Region (L)
P_1	1200	2, 3, ..., 6	2, 3, ..., 10
P_2	1200	7, 8, ..., 10	11, 12, ..., 18
P_3	1200	11, 12, ..., 14	19, 20, ..., 26

TABLE V

COMPARISON OF THE METHODS FOR SPLICING LOCALIZATION IN THE IMAGES WITH VARIOUS BLUR DEGREES DEFINED IN DATASETS P_1 TO P_3

Method	Datasets	TPR(%)	TNR(%)	Accuracy(%)
Su *et al.* [33]	P_1	79.2	77.2	77.3
	P_2	76.4	78.3	78.2
	P_3	82.2	79.5	79.6
	$P_1 + P_2 + P_3$	81.8	78.3	78.4
Chen *et al.* [35]	P_1	81.3	82.7	82.6
	P_2	83.2	80.4	80.5
	P_3	82.2	83.9	83.8
	$P_1 + P_2 + P_3$	83.8	81.3	81.4
Aizenburg *et al.* [36]	P_1	79.3	83.5	83.3
	P_2	82.4	84.7	84.6
	P_3	84.3	86.9	86.8
	$P_1 + P_2 + P_3$	83.1	85.3	85.2
Proposed Method	P_1	93.2	93.7	93.6
	P_2	95.1	93.9	94.0
	P_3	94.3	95.2	95.1
	$P_1 + P_2 + P_3$	96.1	94.7	94.8

Table V shows the performance comparison of our method with the prior works [33], [35], [36] when the blurriness is increased from P_1 to P_3 and also for $P_1 + P_2 + P_3$, where all images with different blur degrees are mixed together. The result reveals that our method outperforms others.

2) The Spliced Region Is Blurred by Non-Parametric Blur Kernel: In this case, we assume that the forger uses

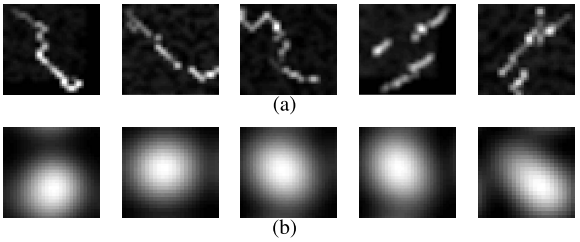

Fig. 9. Examples of non-parametric blur kernels used to blur the sharp spliced region. (a) motion blur (b) out-of-focus blur.

TABLE VI
PERFORMANCE COMPARISON OF THE METHODS FOR SPLICING LOCALIZATION WHEN THE SPLICED REGION HAS COMPLICATED BLURS

Method	Spliced Region Size	TPR (%)	TNR (%)	Accuracy (%)
Chen *et al.* [33]	100×100	57.4	59.5	59.4
	200×200	62.1	57.7	57.9
Su *et al.* [35]	100×100	55.6	61.9	61.8
	200×200	64.2	62.5	62.6
Proposed Method	100×100	91.4	93.2	93.1
	200×200	92.2	94.7	94.6

non-parametric blur kernels (complex form of blur) to blur the tampered region. To evaluate our method, we use 200 non-parametric motion and 200 non-parametric out-of-focus blur kernels with some examples shown in Fig. 9 (a) and (b). We estimate the motion and out-of-focus blur kernels from the blocks of the blurred images of the previous datasets. The location of the blocks is selected at random and the size of blocks is randomly chosen from 64×64 pixels to the whole size of image. Followed by the estimation of the blur kernels, we choose 200 blur kernels which have non-parametric shapes such as motion blur kernels with complicated blur kernel shapes (non-linear, multi line, etc.) and 200 out-of-focus blur kernels with asymmetric shapes. Then, we resize the blur kernels to have different blur degrees for each blur kernel. By resizing the motion blur kernels into sizes of 3×3, 9×9, 15×15, and out-of-focus blur kernels into sizes of 3×3, 7×7, 11×11, we generate 600 non-parametric motion and 600 non-parametric out-of-focus blur kernels, respectively.

We create a dataset of 1200 tampered images using the collected 600 natural motion blurred images and 600 natural out-of-focus blurred images. We insert in each out-of-focus blurred image a sharp region blurred with one of the non-parametric motion blur kernels. We also insert in each motion blurred image a sharp region blurred with one of the non-parametric out-of-focus blur kernels. The 1200 spliced regions are considered as irregular shapes with size of about 100×100 and 200×200, extracted with random spatial alignments from the set of 1200 sharp images used in the previous experiment. Table VI shows the performance comparison of our method with Chen *et al*. [33] and Su *et al*. [35] in splicing localization. The result shows that the prior works have low performance because these methods assume simple shape for the blur kernels. They consider the direction of linear motion blur to classify motion and out-of-focus blurs which is not applicable for these complicated forms. However, our proposed blur type detection features work well even for complicated forms of blur kernels.

VI. CONCLUSIONS AND DISCUSSIONS

In this paper, a new framework was proposed for splicing localization in a spliced blurred image. After partitioning the image into blocks, the local blur type features are extracted. These local features are incorporated for classification of the image blocks into out-of-focus or motion. Finally, based on the human decision, a multiple blur type image is detected as tampered when the motion blurred region is stationary. In such a case, the different blur types indicate the spliced and authentic regions. The experimental results in the partial blur type detection show that the proposed method classifies the out-of-focus and motion blur types successfully, which outperforms the state-of-the-art methods. For more complicated out-of-focus and motion blurs, our proposed feature works well. For forensics application, the evaluation of the proposed method for splicing localization in the tampered images with two blur types (out-of-focus and motion) indicates the efficiency of our method which works well when some post processing operations, such as blurring the spliced boundary and image resizing, are applied after splicing. In such cases, the other techniques are less reliable while our method is robust to such kind of operations. However, it should be noted that when some regions in a tampered image are affected by both out-of-focus and motion blurs, our method cannot resolve such scenario.

In the situation that an anti-forensics person may threat our method, it should be mentioned that detection of blur type by human vision may not be easy, due to the blur degree and image content. However, in the case that an anti-forensics person can detect the partial blur types in different regions. This person may try to deblur these regions to create a consistent blur type. In such a case, since the blur is space-variant across the image, it is difficult to restore the whole image in sharp and blur with a desire blur type. Actually, these operations (deblurring and blurring with another blur type) create strong artifacts in the image which will degrade the quality of the image. In addition, usually image splicing creation involves the incorporation of more than a single technique which leaves these artifacts. An image forensics system based on a certain type of artifact may be attacked with a sophisticated attacker, but covering various tampering detection artifacts is very challenging task.

REFERENCES

[1] S. Dai and Y. Wu, "Motion from blur," in *Proc. IEEE Conf. CVPR*, Jun. 2008, pp. 1–8.
[2] H. Ji and C. Liu, "Motion blur identification from image gradients," in *Proc. IEEE Conf. CVPR*, Jun. 2008, pp. 1–8.
[3] E. Kee, S. Paris, S. Chen, and J. Wang, "Modeling and removing spatially-varying optical blur," in *Proc. IEEE ICCP*, Apr. 2011, pp. 1–8.
[4] R. Fergus, B. Singh, A. Hertzmann, S. T. Roweis, and W. T. Freeman, "Removing camera shake from a single photograph," *ACM Trans. Graph.*, vol. 25, no. 3, pp. 787–794, 2006.

[5] L. Yuan, J. Sun, L. Quan, and H.-Y. Shum, "Blurred/non-blurred image alignment using sparseness prior," in *Proc. IEEE 11th ICCV*, Oct. 2007, pp. 1–8.

[6] J. Chen, L. Yuan, C.-K. Tang, and L. Quan, "Robust dual motion deblurring," in *Proc. IEEE Conf. CVPR*, Jun. 2008, pp. 1–8.

[7] O. Whyte, J. Sivic, A. Zisserman, and J. Ponce, "Non-uniform deblurring for shaken images," in *Proc. IEEE Connf. CVPR*, Jun. 2010, pp. 491–498.

[8] A. Chakrabarti, T. Zickler, and W. T. Freeman, "Analyzing spatially-varying blur," in *Proc. IEEE Conf. CVPR*, Jun. 2010, pp. 2512–2519.

[9] S. Cho and S. Lee, "Fast motion deblurring," *ACM Trans. Graph.*, vol. 28, no. 5, pp. 1–8, 2009.

[10] H. Farid, "Image forgery detection," *IEEE Signal Process. Mag.*, vol. 26, no. 2, pp. 16–25, Mar. 2009.

[11] T. Bianchi and A. Piva, "Image forgery localization via block-grained analysis of JPEG artifacts," *IEEE Trans. Inf. Forensics Security*, vol. 7, no. 3, pp. 1003–1017, Jun. 2012.

[12] P. Ferrara, T Bianchi, A. De Rosa, and A. Piva, "Image forgery localization via fine-grained analysis of CFA artifacts," *IEEE Trans. Inf. Forensics Security*, vol. 7, no. 5, pp. 1566–1577, Oct. 2012.

[13] H. Cao and A. C. Kot, "Accurate detection of demosaicing regularity for digital image forensics," *IEEE Trans. Inf. Forensics Security*, vol. 4, no. 4, pp. 899–910, Dec. 2009.

[14] A. Swaminathan, M. Wu, and K. J. R. Liu, "Digital image forensics via intrinsic fingerprints," *IEEE Trans. Inf. Forensics Security*, vol. 3, no. 1, pp. 101–117, Mar. 2008.

[15] Y.-F. Hsu and S.-F. Chang, "Camera response functions for image forensics: An automatic algorithm for splicing detection," *IEEE Trans. Inf. Forensics Security*, vol. 5, no. 4, pp. 816–825, Dec. 2010.

[16] M. Chen, J. Fridrich, M. Goljan, and J. Lucas, "Determining image origin and integrity using sensor noise," *IEEE Trans. Inf. Forensics Security*, vol. 3, no. 1, pp. 74–90, Mar. 2008.

[17] A. C. Popescu and H. Farid, "Exposing digital forgeries by detecting traces of resampling," *IEEE Trans. Signal Process.*, vol. 53, no. 2, pp. 758–767, Feb. 2005.

[18] B. Mahdian and S. Saic, "Blind authentication using periodic properties of interpolation," *IEEE Trans. Inf. Forensics Security*, vol. 3, no. 3, pp. 529–538, Sep. 2008.

[19] M. C. Stamm and K. J. R. Liu, "Forensic detection of image manipulation using statistical intrinsic fingerprints," *IEEE Trans. Inf. Forensics Security*, vol. 5, no. 3, pp. 492–506, Sep. 2010.

[20] Y. Q. Shi, C. Chen, G. Xuan, and W. Su, "Steganalysis versus splicing detection," in *Proc. 6th Int. Workshop Digit. Watermarking*, 2007, pp. 158–172.

[21] J. Fridrich and J. Kodovsky, "Rich models for steganalysis of digital images," *IEEE Trans. Inf. Forensics Security*, vol. 7, no. 3, pp. 868–882, Jun. 2012.

[22] M. K. Johnson and H. Farid, "Exposing digital forgeries in complex lighting environments," *IEEE Trans. Inf. Forensics Security*, vol. 2, no. 3, pp. 450–461, Sep. 2007.

[23] H. Yao, S. Wang, Y. Zhao, and X. Zhang, "Detecting image forgery using perspective constraints," *IEEE Signal Process. Lett.*, vol. 19, no. 7, pp. 123–126, Mar. 2012.

[24] K. Bahrami, A. C. Kot, and J. Fan, "Splicing detection in out-of-focus blurred images," in *Proc. IEEE Int. WIFS*, Nov. 2013, pp. 144–149.

[25] Y. Sutcu, B. Coskun, H. T. Sencar, and N. Memon, "Tamper detection based on regularity of wavelet transform coefficients," in *Proc. IEEE ICIP*, Sep./Oct. 2007, pp. I-397–I-400.

[26] D. Y. Hsiao and S. C. Pei, "Detecting digital tampering by blur estimation," in *Proc. 1st Int. Workshop Syst. Approaches Digit. Forensic Eng.*, 2005, pp. 264–278.

[27] X.-J. Shen, B.-H. Tang, X.-F. Li, and H.-P. Chen, "A blur image blind identify algorithm based on the edge feature," in *Proc. Int. Conf. Multimedia Inf. Netw. Secur.*, 2011, pp. 309–313.

[28] J. Wang, G. Liu, B. Xu, H. Li, Y. Dai, and Z. Wang, "Image forgery forensics based on manual blurred edge detection," in *Proc. Int. Conf. Multimedia Inf. Netw. Secur.*, 2010, pp. 907–911.

[29] L. Zhou, D. Wang, Y. Guo, and J. Zhang, "Blur detection of digital forgery using mathematical morphology," in *Agent and Multi-Agent Systems: Technologies and Applications*. Berlin, Germany: Springer-Verlag, 2007, pp. 990–998.

[30] G. Cao, Y. Zhao, and R. Ni, "Edge-based blur metric for tamper detection," *J. Inf. Hiding Multimedia Signal Process.*, vol. 1, no. 1, pp. 20–27, 2010.

[31] X. Wang, B. Xuan, and S.-L. Peng, "Digital image forgery detection based on the consistency of defocus blur," in *Proc. Int. Intell. Inf. Hiding Multimedia Signal Process.*, Aug. 2008, pp. 192–195.

[32] P. Kakar, N. Sudha, and W. Ser, "Exposing digital image forgeries by detecting discrepancies in motion blur," *IEEE Trans. Multimedia*, vol. 13, no. 3, pp. 443–452, Jun. 2011.

[33] X. Chen, J. Yang, Q. Wu, J. Zhao, and X. He, "Directional high-pass filter for blurry image analysis," *Signal Process., Image Commun.*, vol. 27, no. 7, pp. 760–771, 2012.

[34] R. Liu, Z. Li, and J. Jia, "Image partial blur detection and classification," in *Proc. IEEE Conf. CVPR*, Jun. 2008, pp. 1–8.

[35] B. Su, S. Lu, and C. L. Tan, "Blurred image region detection and classification," in *Proc. 19th ACM Int. Conf. Multimedia*, 2011, pp. 1397–1400.

[36] I. Aizenberg, D. V. Paliy, J. M. Zurada, and J. T. Astola, "Blur identification by multilayer neural network based on multivalued neurons," *IEEE Trans. Neural Netw.*, vol. 19, no. 5, pp. 883–898, May 2008.

[37] K. Bahrami and A. C. Kot, "Image tampering detection by exposing blur type inconsistency," in *Proc. IEEE ICASSP*, May 2014, pp. 2654–2658.

[38] K. Sharifi and A. Leon-Garcia, "Estimation of shape parameter for generalized Gaussian distributions in subband decompositions of video," *IEEE Trans. Circuits Syst. Video Technol.*, vol. 5, no. 1, pp. 52–56, Feb. 1995.

[39] A. Levin, Y. Weiss, F. Durand, and W. T. Freeman, "Efficient marginal likelihood optimization in blind deconvolution," in *Proc. IEEE Conf. CVPR*, Jun. 2011, pp. 2657–2664.

[40] N. Joshi, R. Szeliski, and D. Kriegman, "PSF estimation using sharp edge prediction," in *Proc. IEEE Conf. CVPR*, Jun. 2008, pp. 1–8.

[41] D. Krishnan, T. Tay, and R. Fergus, "Blind deconvolution using a normalized sparsity measure," in *Proc. IEEE Conf. CVPR*, Jun. 2011, pp. 233–240.

[42] Q. Shan, J. Jia, and A. Agarwala, "High-quality motion deblurring from a single image," *ACM Trans. Graph.*, vol. 27, no. 3, 2008, Art. ID 73.

[43] L. Xu and J. Jia, "Two-phase kernel estimation for robust motion deblurring," in *Proc. 11th ECCV*, 2010, pp. 157–170.

[44] L. Xu and J. Jia, "Depth-aware motion deblurring," in *Proc. IEEE ICCP*, Apr. 2012, pp. 1–8.

[45] G. J. McLachlan, *Discriminant Analysis and Statistical Pattern Recognition*. Hoboken, NJ, USA: Wiley, 2004.

[46] R. Ferzli and L. J. Karam, "A no-reference objective image sharpness metric based on the notion of just noticeable blur (JNB)," *IEEE Trans. Image Process.*, vol. 18, no. 4, pp. 717–728, Apr. 2009.

[47] A. Levin, D. Lischinski, and Y. Weiss, "A closed-form solution to natural image matting," *IEEE Trans. Pattern Anal. Mach. Intell.*, vol. 30, no. 2, pp. 228–242, Feb. 2008.

[48] *Flicker Website*. [Online]. Available: http://www.flicker.com, accessed Aug. 2014.

Khosro Bahrami received the B.Sc. degree in computer engineering from Shiraz University, Shiraz, Iran, in 2000, and the M.Sc. degree in computer engineering from the Sharif University of Technology, Tehran, Iran, in 2002. He is currently pursuing the Ph.D. degree with the Rapid-Rich Object Search Laboratory, School of Electrical and Electronic Engineering, Nanyang Technological University, Singapore. His research interests include image quality assessment, image enhancement, computer vision, and image forensics.

Mr. Bahrami served as a reviewer for the IEEE TRANSACTIONS ON IMAGE PROCESSING, the IEEE TRANSACTIONS ON INFORMATION FORENSICS AND SECURITY, and the IEEE TRANSACTIONS ON CYBERNETICS.

Alex C. Kot (F'06) has been with Nanyang Technological University, Singapore, since 1991. He headed the Division of Information Engineering at the School of Electrical and Electronic Engineering for eight years and served as Associate Chair/Research and Vice Dean Research for the School of Electrical and Electronic Engineering. He is a Professor and an Associate Dean of the College of Engineering and the Director of the Rapid-Rich Object Search Laboratory with Nanyang Technological University. He has published extensively in the areas of signal processing for communication, biometrics, data hiding, image forensics, information security, and image object retrieval and recognition.

Dr. Kot served as an Associate Editor of the IEEE TRANSACTIONS ON SIGNAL PROCESSING, the IEEE TRANSACTIONS ON MULTIMEDIA, the IEEE SIGNAL PROCESSING LETTERS, the *IEEE Signal Processing Magazine*, the IEEE JOURNAL OF SELECTED TOPICS IN SIGNAL PROCESSING, the IEEE TRANSACTIONS ON CIRCUITS AND SYSTEMS FOR VIDEO TECHNOLOGY, the IEEE TRANSACTIONS ON INFORMATION FORENSICS AND SECURITY, the IEEE TRANSACTIONS ON IMAGE PROCESSING, the IEEE TRANSACTIONS ON CIRCUITS AND SYSTEMS PART II, and the IEEE TRANSACTIONS ON CIRCUITS AND SYSTEMS PART I. He served the IEEE Signal Processing Society in various capacities, such as the General Cochair of the 2004 IEEE International Conference on Image Processing and the Vice President of the IEEE Signal Processing Society. He received the Best Teacher of the Year Award, and is a coauthor of several best paper awards, including ICPR, the IEEE WIFS, and IWDW. He is the IEEE Distinguished Lecturer of the Signal Processing Society and a fellow of the Institution of Engineers and the Academy of Engineering, Singapore.

Leida Li received the B.S. and Ph.D. degrees from Xidian University, Xi'an, China, in 2004 and 2009, respectively. In 2008, he was a Research Assistant with the Department of Electronic Engineering, National Kaohsiung University of Applied Sciences, Kaohsiung, Taiwan. From 2014 to 2015, he was a Visiting Research Fellow with the School of Electrical and Electronic Engineering, Nanyang Technological University, Singapore. He is currently an Associate Professor with the School of Information and Electrical Engineering, China University of Mining and Technology, Xuzhou, China. His research interests include multimedia quality assessment, information hiding, and image forensics.

Haoliang Li received the B.S. degree from the University of Electronic Science and Technology of China, Chengdu, China, in 2013. He is currently pursuing the Ph.D. degree with the Rapid-Rich Object Search Laboratory, Nanyang Technological University, Singapore. His research interests include multimedia forensics and computer vision.